ORIGINAL ARTICLE

Modeling and simulation of workpiece surface flatness in magnetorheological plane finishing processes

Zhanbin Liu[1] · Jianyong Li[1] · Meng Nie[1] · Yueming Liu[1]

Abstract

Multi-pole arrangements in magnetorheological plane finishing technology have been investigated in this study. A method of combining the material removal mechanism of micro-points using the empirical Preston equation is proposed to establish a prediction model for surface flatness, and the new Semiconductor Equipment and Materials International (SEMI) standard has been used to evaluate workpiece surface flatness. Based on the model, the effects of process parameters (polishing time, speed ratio, translational amplitude, polishing gap, etc.) on the flatness of workpieces with different shapes are predicted through simulation, and the effects of multi-pole arrangements are explored. The results of the analysis indicate that with changes in process parameters, the extent of change in surface flatness differs based on the shape of the workpiece. After polishing, concave workpieces show the highest levels of surface flatness. From simulations of magnetic pole arrangements, it is also found that magnetic field generators with different magnetic pole arrangements can be used for workpieces with different shapes to improve their surface flatness. Experiments with a workpiece with its shape measured using a white light interferometer showed that the surface flatness improved from being 33.561 μm initially to 21.822 μm after polishing, thereby demonstrating the effectiveness of the proposed method.

Keywords Magnetorheological plane finishing · Flatness · Process parameters · Multi-pole arrangement

1 Introduction

In recent years, with the rapid development of precision manufacturing, the production and processing of workpieces is subject to increasingly strict requirements for surface quality control, which require surfaces to be of extremely high smoothness, cleanliness, and flatness [1–3]. Flat finishing is the final process of workpiece surface processing and is the key to determining the quality of the workpiece surface. Magnetorheological finishing (MRF) has proven to be an extremely effective technique for ultra-smooth and low-damage processing of workpieces. It relies mainly on the rheological properties of a magnetorheological fluid under the action of a magnetic field to carry abrasive particles that perform material removal [4–6]. The finishing medium of MRF is in flexible

contact with the processed object. It is characterized by a low normal pressure, which does not easily cause surface and subsurface damages and can control the amount of material removed [7, 8]. It has been used to achieve precision finishing of non-magnetic materials, such as optical components, ceramic devices, stainless steel, and semiconductors, and has achieved remarkable results in several finishing processes [9–11]. Relevant research studies [12–14] show that MRF can achieve extremely low surface roughness and has the potential for application in the industrial finishing of workpieces, but it is difficult to achieve efficient planarization due to the characteristic of having an overall flexible contact.

To improve wafer flatness, Wang et al. [15] proposed the addition of translational motion to the process of magnetorheological finishing. Zhang et al. [16] proposed a new reciprocating magnetorheological (MR) method for flat finishing the surface of borosilicate glass. Fang et al. [17] studied the effect of the distribution of abrasives in the polishing pad on the uniformity and roughness of the workpiece surface. The results show that the thickness of the workpiece surface changes by about 2.8 μm when a conventional polishing pad is used for polishing, compared with a change of

✉ Meng Nie
nmbc@bjtu.edu.cn

1   School of Mechanical, Electronic and Control Engineering, Beijing Jiaotong University, Beijing 100044, China

about 1.8 μm when a polishing pad with radially distributed abrasives is used. Thus, polishing pads with radially distributed abrasives can achieve better surface uniformity and roughness than conventional polishing pads. Krishnan et al. [18] adopted MRF for local finishing and reported that it achieved flatness correction with a longer duration of application on the *high point* than on the *low point*, and obtained a high flatness improvement rate with each finishing iteration. Nie et al. [19] proposed a clustered magnetic field magnetorheological finishing method based on a leaf order mode. Theoretically, an optimum magnet arrangement can achieve a higher finishing efficiency and better wafer flatness. Guan et al. [20] proposed a new MRF method, called LAP-MRF. They used a finite element analysis method to simulate the permanent magnet unit, and a multi-parameter optimization was performed to effectively improve the flatness of a wafer.

Although processing technology is constantly improving and being perfected and the flatness of workpieces is reaching higher levels of precision, current technology and methods are unable to meet production needs [21]. Therefore, the establishment of a predictive model for workpiece surface flatness will provide theoretical support and implementation methods for achieving high-efficiency, high-flatness, and ultra-smooth workpiece surfaces using magnetorheological plane finishing processes, and these are thus of important practical

significance in improving the finishing efficiency and quality of workpieces. This paper proposes a method that incorporates the material removal mechanism of micro-points in the empirical Preston equation to establish a prediction model for workpiece surface flatness and simulates the effect of process parameters and magnetic pole arrangements on the surface flatness of workpieces with different shapes.

2 The principle of magnetorheological plane finishing

A schematic diagram of the magnetorheological plane finishing (MRPF) apparatus is illustrated in Fig. 1. A magnetorheological polishing liquid is placed above the polishing disk, and a magnetic field generator is placed below the polishing disk. In the area of the polishing disk directly above the magnetic field generator, magnetic particles in the magnetorheological polishing fluid get arranged in a chain-like manner along the direction of the magnetic field lines due to the action of the magnetic field; the abrasive particles in the polishing fluid get mixed into the magnetic chains and are carried and constrained by the magnetic particles. The magnetorheological polishing liquid forms a flexible polishing film with the rigidity and strength necessary to
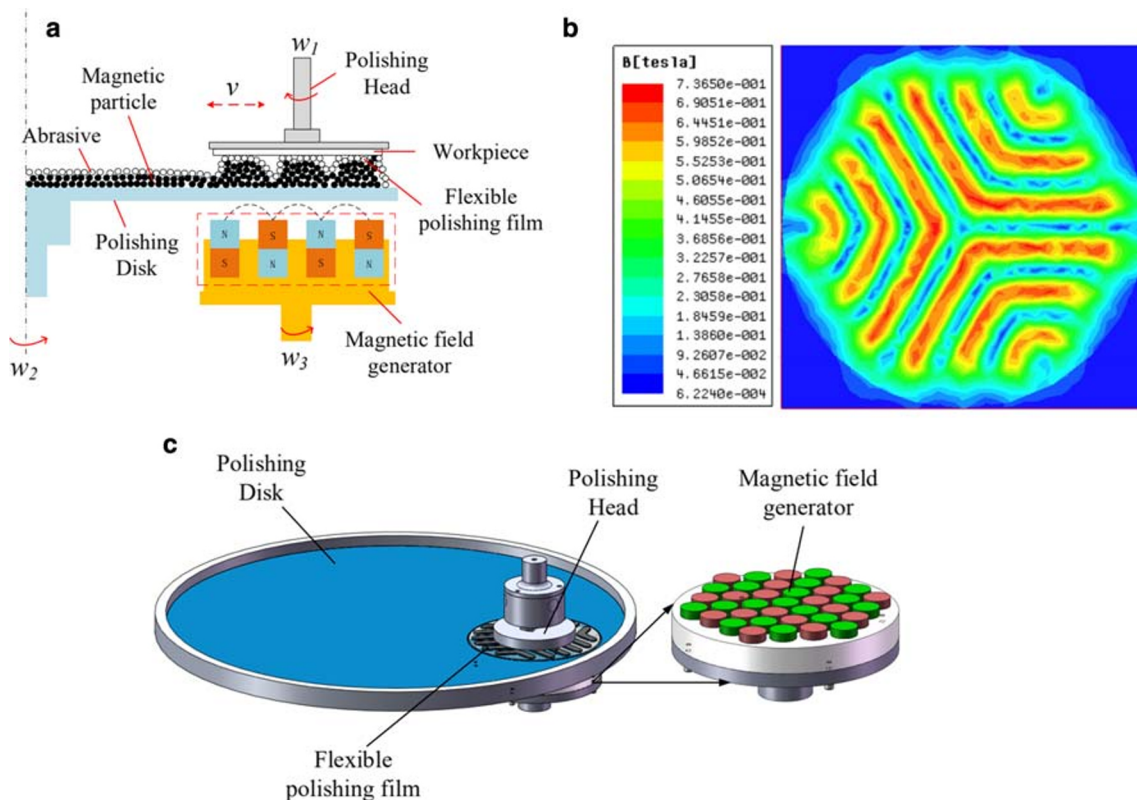
Fig. 1 Schematic diagram of MRPF. **a** MRPF schematic diagram. **b** Magnetic flux density at the processing gap of 2 mm. **c** MRPF three-dimensional map

polish the workpiece above the polishing disk. When the polishing disk, the polishing head in contact with the workpiece, and the magnetic field generator rotate due to the turning of the motor, the flexible polishing film will then move relative to the workpiece, thereby removing material. Besides, the rotation of the magnetic field generator allows the flexible polishing film to be corrected in real time and updated to self-sharpen, enabling better material removal.

Based on the above principles of magnetorheological plane finishing, it is assumed that abrasive particles and magnetic particles are in a circular motion along with the rotation of the polishing disk, and the rotation of the magnetic field generator only causes the particles in the magnetic field polishing area to move up and down along magnetic force lines; hence, the relative speed of the workpiece surface is obtained by combining the speeds of the polishing disk and the workpiece. The positive polishing force on the workpiece surface is provided by the magnetorheological polishing pad generated by the magnetic field generator. As can be seen from Fig. 1c, a magnetorheological flexible polishing film is formed directly above the magnetic field generator. Its characteristics are directly determined by the magnetic field generator which is the main factor affecting the polishing quality and efficiency of the workpiece. Ansoft Maxwell software is used to simulate and analyze the magnetic flux density of the polishing gap at 2 mm, as shown in Fig. 1b; it can be seen that the flexible polishing film is distributed as a magnetic pole arrangement.

3 Modeling of surface flatness

To understand the effects of different magnetic pole arrangements and process parameters (polishing time, speed ratio, deflection speed, processing gap, etc.) on workpiece surface flatness, it is necessary to establish a predictive model of surface flatness during the MRPF process. It is proposed that a method of combining the mechanism of removal of micropoints with the empirical Preston equation be used for this purpose. The MRPF process requires a certain polishing speed and positive polishing pressure in the magnetic field polishing area and uses abrasive particles to remove material from the surface of the workpiece. The amount of material removed from the workpiece surface is obtained from the Preston formula, expressed as

$$MRR = KPVT \qquad (1)$$

where MRR is the amount of material removed from the workpiece surface; K is the Preston coefficient, which is based on the effect of parameters other than pressure and speed on the amount of material removed and is obtained from experimentation; P is the positive polishing pressure on the workpiece surface; V is the relative speed of the workpiece surface and

the polishing disk; and T is the polishing time.

From Eq. (1), it can be seen that the positive polishing pressure is one of the main parameters for material removal on the workpiece surface and is also the main parameter that affects the quality of the workpiece surface. During the polishing process, the motion of the abrasive particles is not influenced by the magnetic force in the magnetic field but relies mainly on the magnetic chain generated by the magnetic field in which the particles are entrapped and carried with, to facilitate the removal of material on the workpiece surface. Therefore, the positive pressure of the magnetic particles on the workpiece surface can be approximated as being the positive pressure on the processed surface [22]. The positive pressure generated by the magnetic particles in the magnetorheological polishing fluid on the surface of the workpiece involves several complexities. Hence, the following simplifying assumptions are made for analyzing the force on the workpiece: (1) the magnetic particle force model is simplified in two-dimensional space, which is based on the force analysis of the uppermost particles of the magnetorheological polishing fluid in contact with the workpiece surface; (2) the presence of abrasive particles does not affect the formation of the magnetic chain, and these particles are evenly distributed in the polishing solution; (3) the model ignores the van der Waals and Brownian forces between particles and the adhesion of fluid to the particles; and (4) the model ignores the effect of the magnetizing field generated by the magnetic particles on the magnetic field from the magnetic field generator.

Figure 2 shows the model used for the analysis of the force acting on the surface of the workpiece. The equation for the positive polishing force generated by the magnetic particles on the workpiece surface is as follows:

$$Pn = Pm + Pd + Pb - Pg \qquad (2)$$

where Pn is the resultant positive polishing force, Pm is the force due to the magnetic field gradient, Pd is the hydrodynamic force of the magnetorheological polishing fluid, Pb is the buoyancy of particles, and Pg is the weight of the particles. Since the weight and buoyancy of the particles are very small compared to other forces, they are neglected for this analysis.

Pan and Yan [23] pointed out that hydrodynamic pressure only exists at the edge of the wafer and only before the workpiece is in complete contact with the magnetorheological polishing fluid for a very short duration. The material removed from the surface of the workpiece surface occurs mainly after the workpiece is in complete contact with the polishing fluid; therefore, the force resulting from the hydrodynamic pressure is ignored during the polishing process; that is, the positive polishing force on the workpiece is equal to the force due to the magnetic field [24]. The distribution of the positive polishing force field can be obtained by substituting the physical parameters of the magnetorheological polishing fluid listed in Table 1 into Eq. (4)

Fig. 2 Model of the forces acting on the workpiece surface
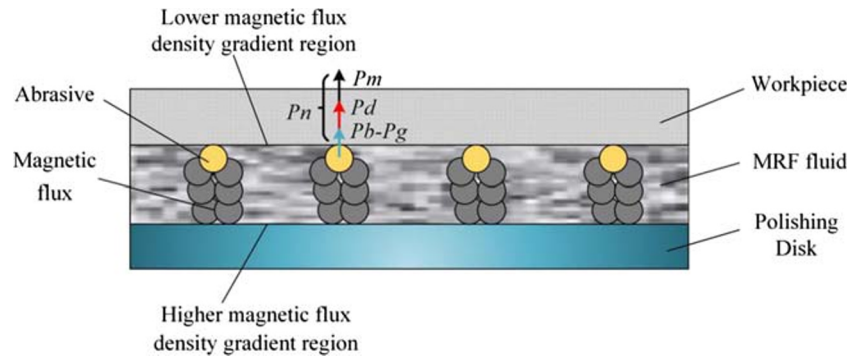
$$Pn = Pm \qquad (3)$$

$$Pm = V0\chi\mu0H\Delta H \qquad (4)$$

where V_0 is the volume of magnetic particles, χ is the magnetic susceptibility of the magnetic particles, μ_0 is the magnetic permeability of free space, H is the magnetic field strength, and ΔH is the gradient of the magnetic field strength.

From an analysis based on the principles of magnetorheological plane finishing, it was found that the removal of material from the workpiece is limited to the magnetic field area of the polishing disk in MRPF. The trajectory of motion of the micro-points on the workpiece surface in the magnetic field region is essentially that of the positive polishing force. In MRPF, the relative speed of the workpiece is obtained by combining the speed of the workpiece and the polishing disk. Therefore, the equation of the trajectory of the micro-points on the workpiece surface relative to the polishing disk can be differentiated with respect to time to obtain the relative speed of the micro-points on the workpiece surface.

The following analysis establishes the equation of the trajectory of motion of the micro-points on the workpiece surface relative to the magnetic field area and the polishing disk and obtains the speed and the positive polishing force of each micro-point on the workpiece surface as a function of time. The Preston formula of the micro-points is thereafter used to get the amount of material removed at all micro-points on the workpiece surface.

Based on the above, a schematic diagram of the movement of the workpiece relative to the polishing disk and the

Table 1 Physical parameters of MRF fluid

Parameters	Value
Average particle size of carbonyl iron (μm)	5
Relative magnetic permeability of carbonyl iron, μ_e	2000
Magnetic permeability of free space, μ_0 (N/A)	$4\pi \times 10^{-7}$
Magnetic field strength (H)	Simulation value

magnetic field area is established for MRPF, as shown in Fig. 3. In Fig. 3a, $x_1o_1y_1$ is a fixed coordinate system with the origin at the center of the workpiece, and $x_2o_2y_2$ is a dynamic coordinate system with the origin at the center of the polishing disk that rotates with the polishing disk; w_1 is the rotational speed of the workpiece, and w_2 is the rotational speed of the polishing disk. The initial position of any point (P) on the workpiece is [$r\cos\varphi$, $r\sin\varphi$] in the coordinate system, and the distance between the workpiece origin and the polishing disk origin is e_1. The equation of the trajectory of the point P in the $x_1o_1y_1$ coordinate system is as follows [25–27]:

$$\begin{bmatrix} x_1 \\ y_1 \end{bmatrix} = \begin{bmatrix} r\cos(\phi + w_1 t) \\ r\sin(\phi + w_1 t) \end{bmatrix} \qquad (5)$$

The conversion relationship between the dynamic coordinate system ($x_2o_2y_2$) and the fixed coordinate system ($x_1o_1y_1$) is as follows:

$$\begin{bmatrix} x_1 \\ y_1 \end{bmatrix} = \begin{bmatrix} \cos(w_2 t) & -\sin(w_2 t) \\ \sin(w_2 t) & \cos(w_2 t) \end{bmatrix} \begin{bmatrix} x_2 \\ y_2 \end{bmatrix} + \begin{bmatrix} -e_1 \\ 0 \end{bmatrix} \qquad (6)$$

Substituting Eq. (5) into Eq. (6), the equation of the trajectory of the point P on the workpiece relative to polishing disk can be derived, as shown in the following equation:

$$\begin{bmatrix} x_2 \\ y_2 \end{bmatrix} = \begin{bmatrix} \cos(w_2 t) & \sin(w_2 t) \\ -\sin(w_2 t) & \cos(w_2 t) \end{bmatrix} \left(\begin{bmatrix} x_1 \\ y_1 \end{bmatrix} - \begin{bmatrix} -e_1 \\ 0 \end{bmatrix} \right) \qquad (7)$$

Equation (7) is differentiated with respect to time to obtain the speed of the point P on the workpiece, as shown in the following equation:

$$\begin{bmatrix} vx_2 \\ vy_2 \end{bmatrix} = \begin{bmatrix} r(w_2-w_1)\sin(w_1 t + \phi - w_2 t) - e_1 w_2 \sin(w_2 t) \\ r(w_1-w_2)\cos(w_1 t + \phi - w_2 t) - e_1 w_2 \cos(w_2 t) \end{bmatrix} \qquad (8)$$

In Fig. 3b, $x_1o_1y_1$ is a fixed coordinate system with the origin at the center of the workpiece, and $x_3o_3y_3$ is a dynamic coordinate system with the origin at the center of the magnetic field area that rotates with the magnetic field area; w_1 is the

Fig. 3 Schematic diagram of workpiece motion in MRPF. Schematic diagram of the relative motion of **a** the workpiece and polishing disk and **b** the workpiece and magnetic field area

(a)   (b)
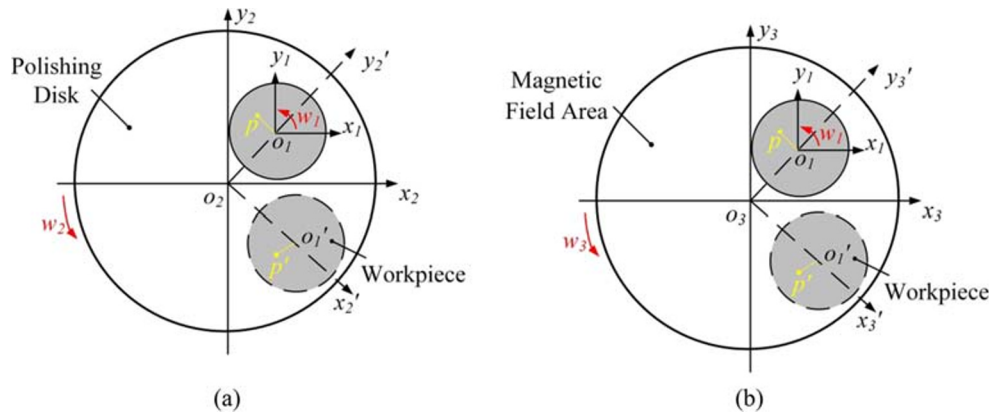
rotational speed of the workpiece, and w_3 is the rotational speed of the magnetic field area. The initial position of any point (P) on the workpiece is [$r\cos\varphi$, $r\sin\varphi$] in the coordinate system, and the distance between the workpiece origin and the polishing disk origin is e_1. The equation of the trajectory of the point P in the $x_1 o_1 y_1$ coordinate system is as follows:

$$\begin{bmatrix} x_1 \\ y_1 \end{bmatrix} = \begin{bmatrix} r\cos(\phi + w_1 t) \\ r\sin(\phi + w_1 t) \end{bmatrix} \tag{9}$$

The conversion relationship between the dynamic coordinate system $x_3 o_3 y_3$ and the fixed coordinate system $x_1 o_1 y_1$ is as follows:

$$\begin{bmatrix} x_1 \\ y_1 \end{bmatrix} = \begin{bmatrix} \cos(w_3 t) & -\sin(w_3 t) \\ \sin(w_3 t) & \cos(w_3 t) \end{bmatrix} \begin{bmatrix} x_3 \\ y_3 \end{bmatrix} + \begin{bmatrix} -e_2 \\ 0 \end{bmatrix} \tag{10}$$

Substituting Eq. (9) into Eq. (10), the equation of the trajectory of the point P on the workpiece relative to the magnetic field area can be derived, as shown in the following equation:

$$\begin{bmatrix} x_3 \\ y_3 \end{bmatrix} = \begin{bmatrix} \cos(w_3 t) & \sin(w_3 t) \\ -\sin(w_3 t) & \cos(w_3 t) \end{bmatrix} \left(\begin{bmatrix} x_1 \\ y_1 \end{bmatrix} - \begin{bmatrix} -e_2 \\ 0 \end{bmatrix} \right) \tag{11}$$

The positive polishing force of the micro-points with time can be obtained from the equation of the trajectory of motion of the micro-points on the workpiece surface and the distribution of the positive polishing force in the magnetic field area.

Based on the above, when the translation between the workpiece and the polishing disk occurs, the schematic diagram of the movement of the workpiece relative to the polishing disk and the magnetic field area is established in MRPF, as shown in Fig. 4. The coordinate system setup, in this case, is consistent with the coordinate system shown in Fig. 4, where V is the translational speed of the workpiece, A is the translational amplitude, and β is the deflection angle. The equation of the trajectory of motion of point P relative to the magnetic field area is as follows:

$$\begin{bmatrix} x_3 \\ y_3 \end{bmatrix} = \begin{bmatrix} \cos(w_3 t) & \sin(w_3 t) \\ -\sin(w_3 t) & \cos(w_3 t) \end{bmatrix} \tag{12}$$
$$\left(\begin{bmatrix} x_1 \\ y_1 \end{bmatrix} - \begin{bmatrix} -(e_2 + (A\sin(\pi v t/2A)\cos\beta)) \\ -A\sin(\pi v t/2A)\sin\beta \end{bmatrix} \right)$$

The equation of the trajectory of motion of point P relative to the polishing disk is as follows:

Fig. 4 Schematic diagram of workpiece motion in MRPF. **a** Schematic diagram of the relative motion of the workpiece and polishing disk. **b** Schematic diagram of the relative motion of the workpiece and magnetic field area

(a)   (b)
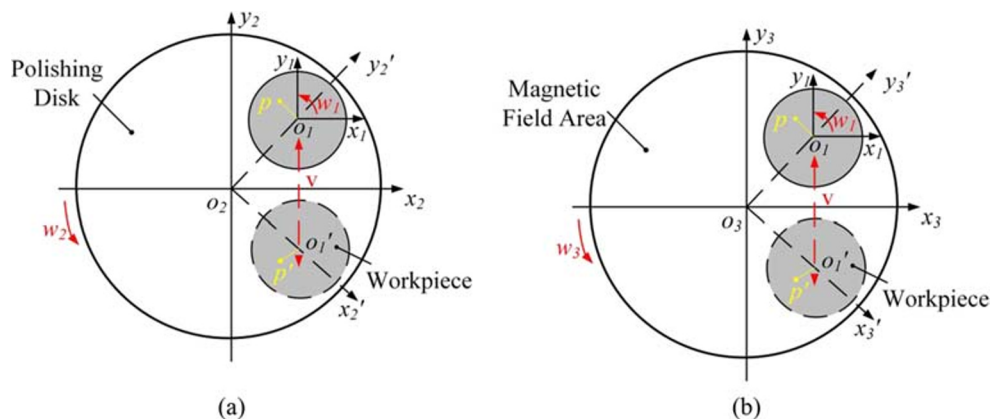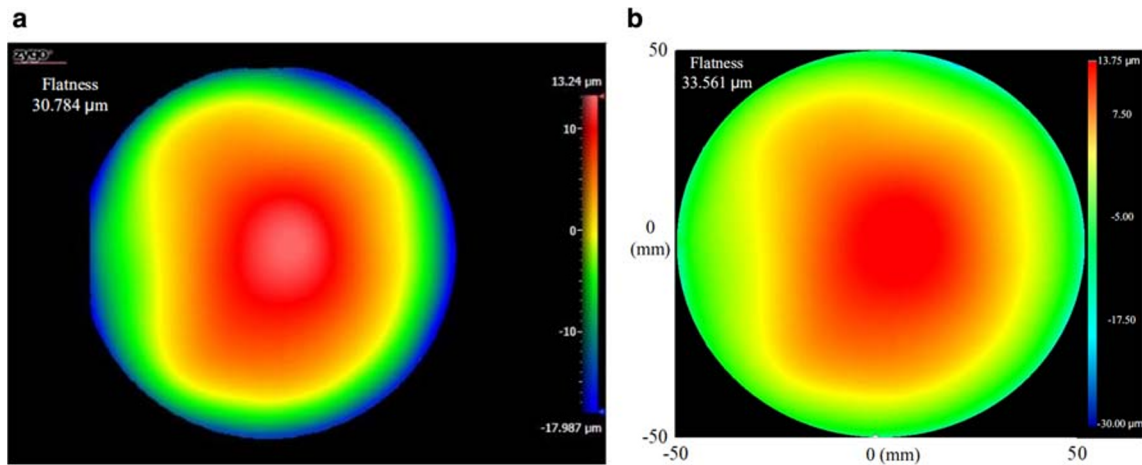
Fig. 5 Extraction of initial topographic features of the workpiece surface. **a** Morphology measured by a white light interferometer. **b** Morphology obtained by data interpolation

$$\begin{bmatrix} x_2 \\ y_2 \end{bmatrix} = \begin{bmatrix} \cos(w_2 t) & \sin(w_2 t) \\ -\sin(w_2 t) & \cos(w_2 t) \end{bmatrix} \tag{13}$$
$$\left(\begin{bmatrix} x_1 \\ y_1 \end{bmatrix} - \begin{bmatrix} -(e_1 + (A\sin(\pi vt/2A)\cos\beta)) \\ -A\sin(\pi vt/2A)\sin\beta \end{bmatrix} \right)$$

Therefore, the equation for the velocity of point P with time is as follows:

$$\begin{bmatrix} vx_2 \\ vy_2 \end{bmatrix} = \begin{bmatrix} \mathrm{d}(x_2)/\mathrm{d}t \\ \mathrm{d}(y_2)/\mathrm{d}t \end{bmatrix} \tag{14}$$

Therefore, the amount of material removed at any micro-point (P) on the surface of the workpiece is the sum of the corresponding amount of material removed at all points that are the trajectory points of micro-point P relative to the magnetic field area at time T. The amount of material removed at the micro-point P on the workpiece at any time (T) is obtained as follows:

$$MRR_P = \sum_0^T KP_i V_i \tag{15}$$

where MRR_P is the amount of material removed at the micro-point P, T is the polishing time, K is the Preston coefficient, and P_i and V_i are the positive polishing force and relative speed of the workpiece surface and the polishing disk, respectively, at a certain point in time. Subtracting the data set of the amount of material removed at N micro-points on the workpiece surface from the corresponding data set (H_0) of the initial shape of the workpiece surface, the predicted shape of the workpiece surface can be obtained, as shown in the following equation:

$$H = H_0 - \left[\sum_0^T KP_i V_i \right] N \tag{16}$$

where H is the data set of the predicted shape of the workpiece surface, H_0 is the corresponding data set of the initial shape of the workpiece surface, N is the number of micro-points on the workpiece surface, and the remaining variables are consistent with Eq. (15). Next, the evaluation method adopts the new SEMI standard to evaluate the workpiece surface flatness. The global flatness back ideal range (GBIR) is defined as the standard SEMI term, and the total
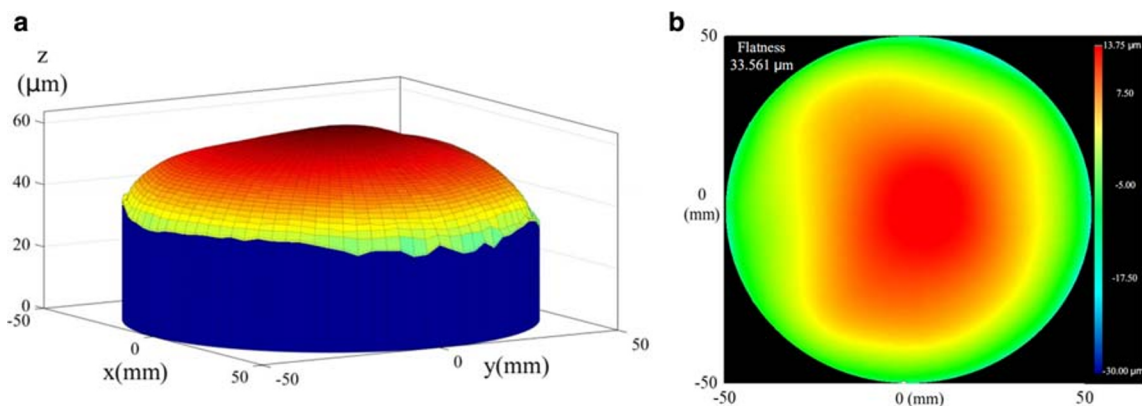
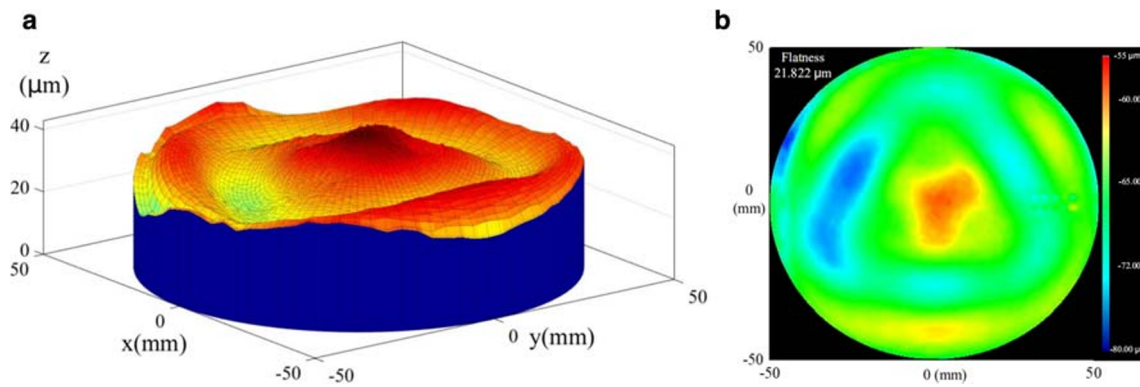**Fig. 6** Model before MRPF. **a** Three-dimensional map. **b** Workpiece surface TTV value

Fig. 7 Model after MRPF. **a** Three-dimensional map. **b** Workpiece surface TTV value

thickness variation (TTV) is designated as the idiomatic term, which is defined as the difference between the highest peak (a) and the lowest valley (b) of the wave surface peak-to-valley value (TTV = $a - b$). Thus, a mathematical model for predicting the workpiece surface flatness can be established as follows:

$$TTV = \max\left(H_0 - \left[\sum_0^T KP_iV_i\right]N\right) - \min\left(H_0 - \left[\sum_0^T KP_iV_i\right]N\right) \tag{17}$$

4 Simulation and analysis

4.1 The simulation of surface flatness

The prediction model for workpiece flatness is established from simulated MRPF processes. The initial surface flatness data of the model was extracted from a white light interferometer at the same intervals of the coordinates of all sampling points in the contour. Since the data measured by the interferometer is the absolute height of the workpiece surface, the least squares method is used to process the original global topography data of the workpiece surface to correct the graphics obtained from Matlab software, as shown in Fig. 5. It can be seen from the figure that the shape of the workpiece obtained by fitting the raw data measured by the white light interferometer is approximately the same as that obtained from actual measurements. The actual measured global flatness is 30.784 μm, compared to the fitted global flatness of 33.561 μm. Thus, the difference between these two values is small. The reason for the difference is that portions of the left and top corners of the actual workpiece morphology are missing in Fig. 5a. However, the original data has been processed and interpolated to fill in the missing portions to obtain the entire workpiece morphology as shown in Fig. 5b. It is seen that the extracted topography is consistent with the directly measured topography using the

Table 2 Simulation experiment process parameters

| Parameters	Polishing conditions					
	Polishing time	Speed ratio	Translational amplitude	Translational speed	Polishing gap	Translational direction
Polishing time (min)	20–120	25	40	40	2	X-axis
Speed ratio (w_1/w_2)	60	15–40	40	40	2	X-axis
Translational amplitude (mm)	60	25	10–70	40	2	X-axis
Translational speed (mm/s)	60	25	40	20–100	2	X-axis
Polishing gap (mm)	60	25	40	40	1–4	X-axis
Translational direction	60	25	40	40	2	X-axis, Y-axis
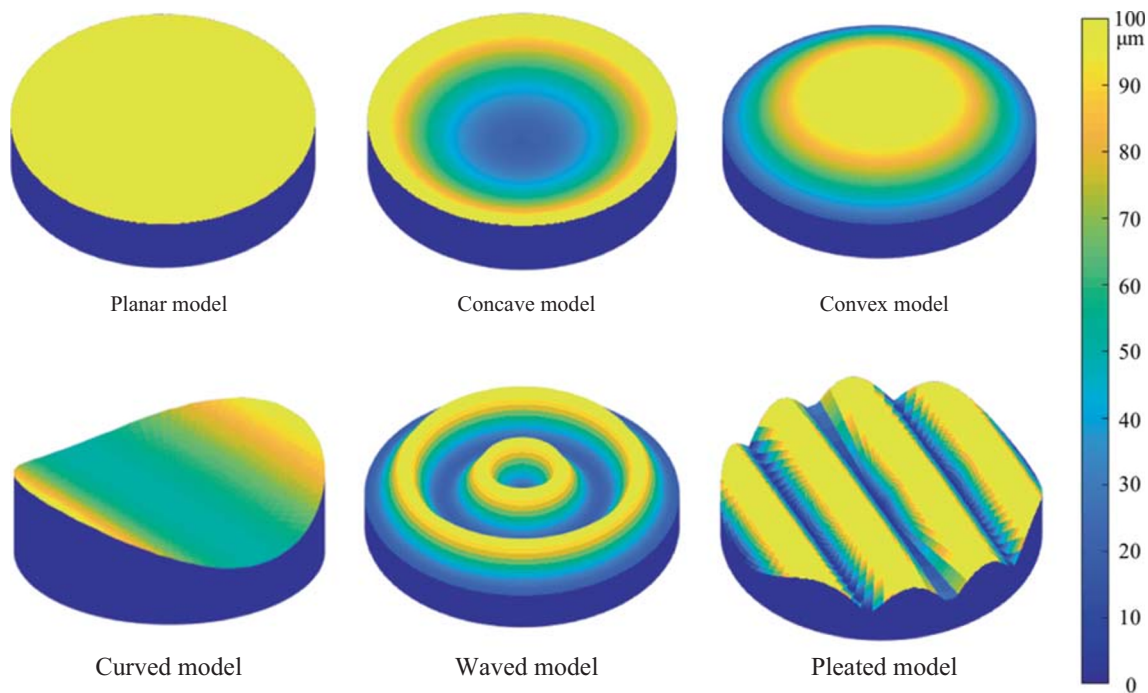
Fig. 8 Workpiece models with different initial shapes

white light interferometer, and that the flatness error does not exceed 3 μm. Hence, the initial shape of the workpiece extracted and processed by Matlab can be considered to be accurate and reliable.

The workpiece with the above initial surface flatness is used as the sample for this study. Under certain polishing process parameters (w_1 = 100 r/min, w_2 = 20 r/min, w_3 = 20 r/min, e_1 = 307.5 mm, e_2 = 70 mm), a predictive model of the morphology of the workpiece is obtained after performing a 150-min simulation experiment. The initial morphology of the workpiece which has a "convex in the middle and concave on both sides" shape is depicted in Fig. 6. After MRPF, the workpiece surface flatness improved from 33.561 to 21.822 μm, as shown in Fig. 7.

4.2 Analysis of the effect of process parameters on flatness

Simulation experiments were conducted to investigate the effects of polishing process parameters (such as polishing time, speed ratio, and polishing gap) on the workpiece surface flatness. The samples used for the simulation are six types of workpiece models with different initial shapes: planar, concave, convex, curved, waved, and pleated. The initial TTV value of the planar shaped model is 0 μm, and the initial TTV value of the other models is 100 μm, as shown in Fig. 8. The parameters for the simulated experiment are shown in Table 2, for which the rotational speed of the polishing disk (w_2) is held constant at 20 r/min.
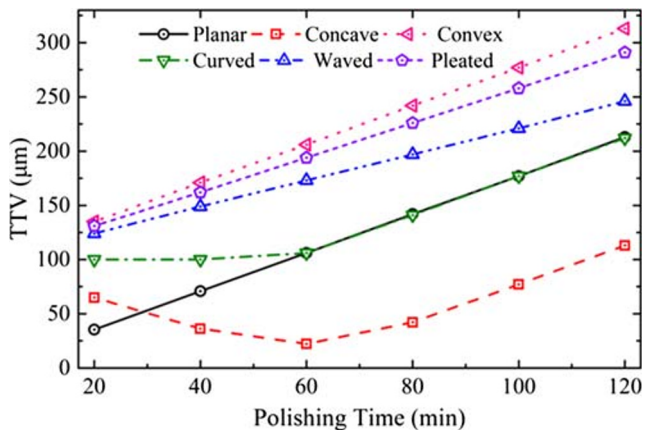

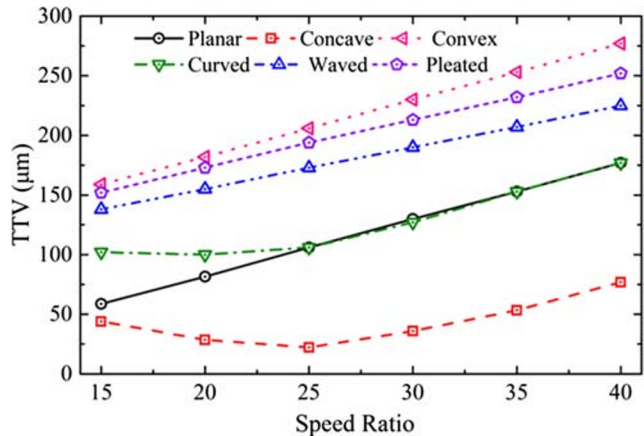**Fig. 9** Relationship between polishing time and TTV

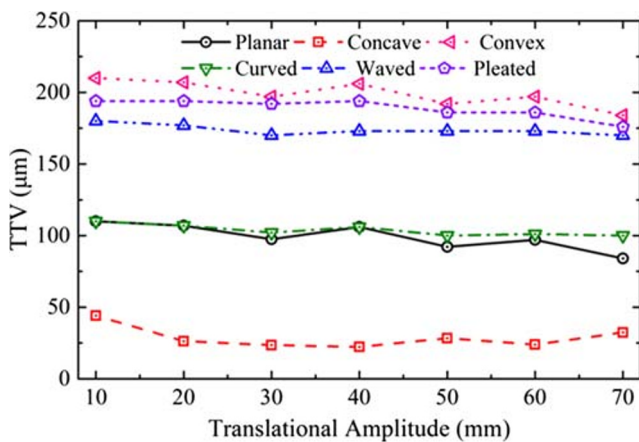**Fig. 10** Relationship between speed ratio and TTV

Fig. 11 Relationship between translational amplitude and TTV

Figure 9 shows the relationship between the polishing time and the TTV value of workpiece surfaces with different initial shapes within the ranges of the simulation parameters. The TTV value of workpiece surfaces with planar, convex, waved, and pleated shapes is proportional to the polishing time. The surface flatness becomes worse with the increase of polishing time. This indicates that these four types of workpieces cannot be corrected for their surface shapes to achieve improved surface flatness for these polishing process parameters.

In the case of the curved workpiece, for a polishing time interval of 0 to 60 min, the surface shape is maintained well and the surface flatness remains unchanged; however, after 60 min, the surface flatness gradually worsens. In the case of the concave workpiece, for a polishing time interval of 0 to 60 min, the surface flatness gradually improves, reaching an optimal state at 60 min with a TTV value of approximately 25 µm; however, between 60 and 120 min, the surface flatness worsens. This indicates that the concave surface flatness improves within a certain polishing time interval but gradually worsens when the polishing time exceeds this interval.

Figure 10 shows the relationship between the speed ratio and the TTV value of workpiece surfaces with different initial shapes. The TTV value of workpiece surfaces with planar,
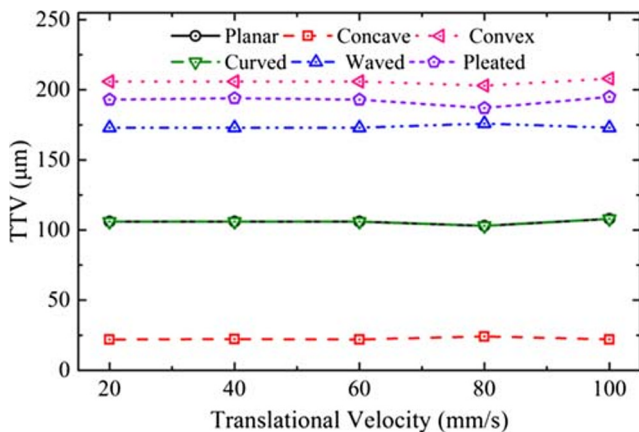
convex, waved, and pleated shapes is proportional to the speed ratio. The surface flatness worsens with an increase in speed ratio. This indicates that these four types of workpieces can be polished for lower speed ratios, which can improve surface flatness, but increasing the speed ratio will worsen the surface flatness.

In the case of the curved workpiece, for the speed ratio ranging from 15 to 25, the surface shape is maintained well and the surface flatness remains unchanged; however, for speed ratios exceeding 25, the surface flatness worsens sharply. In the case of the concave workpiece, for the speed ratio ranging from 15 to 25, the TTV value of the surface is inversely related to the speed ratio; that is, the TTV value becomes smaller and the surface flatness become better with increasing speed ratios; when the speed ratio ranges from 25 to 40, the TTV value of surface is positively related to the speed ratio; that is, the TTV value becomes larger and the surface flatness worsens with increasing speed ratios. This indicates that a certain high value of the speed ratio can improve the flatness of a concave surface.

Figure 11 shows the relationship between the translational amplitude and the TTV value of workpiece surfaces with different initial shapes. For convex and planar workpieces, the TTV value decreases in a wavy manner with an increase in

Fig. 13 Relationship between polishing gap and TTV

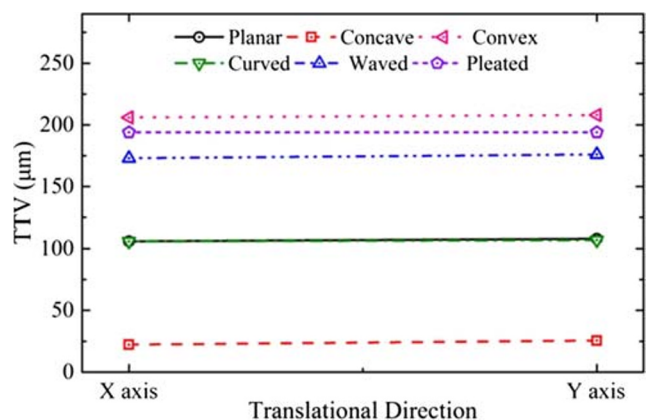Fig. 12 Relationship between translational velocity and TTV

Fig. 14 Relationship between translational direction and TTV

Fig. 15 Model of magnetic field generators with different magnetic pole arrangements. **a** A-shape with the adjacent arrangement of rectangular anisotropic magnetic poles. **b** B-shape with the adjacent arrangement of circular anisotropic magnetic poles. **c** C-shape with the rotating arrangement of cylindrical anisotropic magnetic poles. **d** D-shape with the staggered arrangement of cylindrical anisotropic magnetic poles
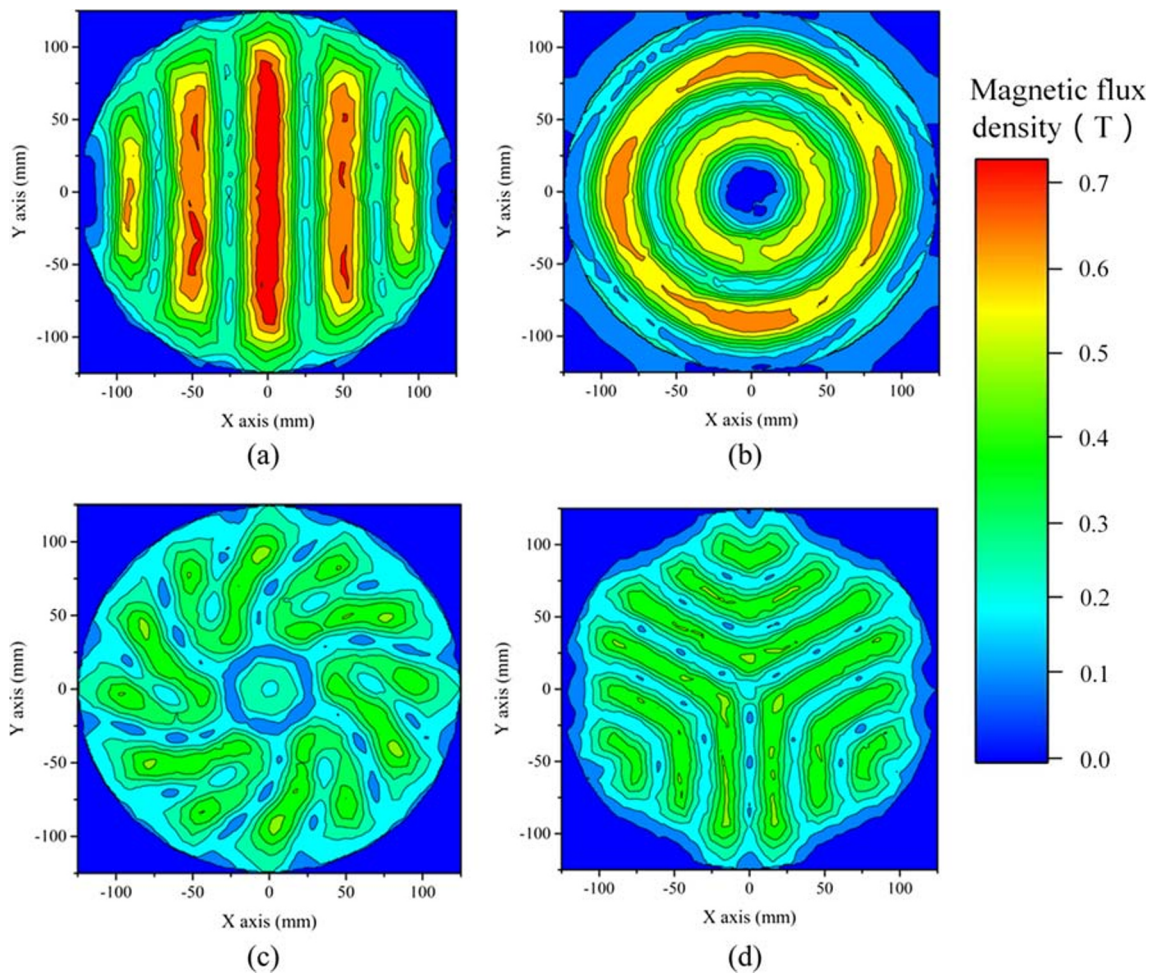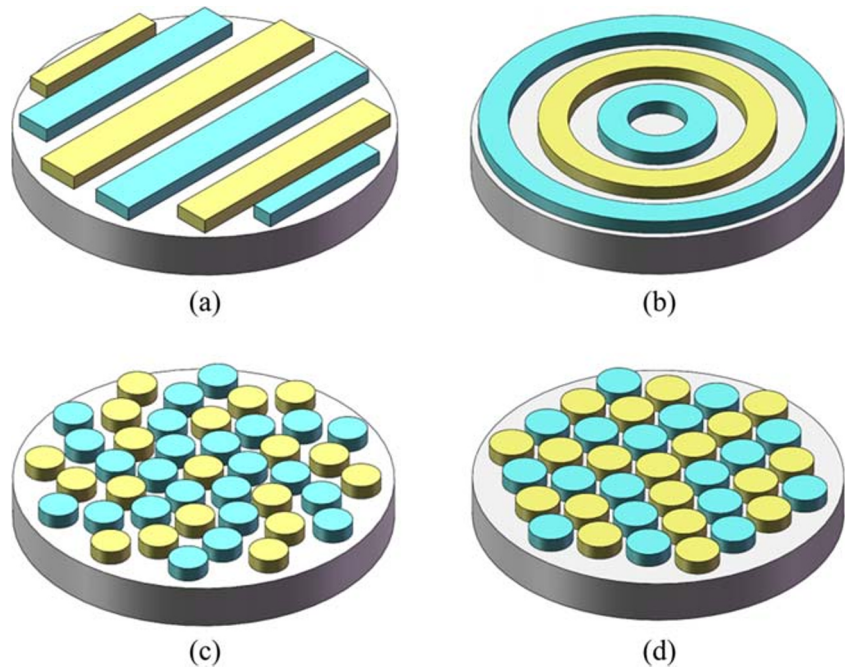
Fig. 16 Simulation of magnetic field strength with different magnetic pole arrangements. **a** A-shape. **b** B-shape. **c** C-shape. **d** D-shape
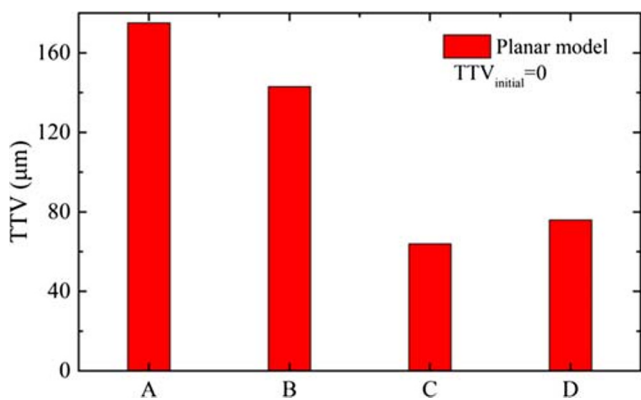
Fig. 17 Effect of different magnetic pole arrangements on the TTV value of planar surfaces

Fig. 19 Effect of different magnetic pole arrangements on the TTV value of a curved surface

translational amplitude. For pleated workpieces, when the translational amplitude ranges from 10 to 40 mm, the relationship between the amplitude and the TTV value of the surface flatness is a horizontal line; that is, the amplitude within this range has little effect on the surface flatness. In the translational amplitude range of 40 to 70 mm, the surface flatness improves with increasing amplitude.

For waved and curved workpieces, the translational amplitude has little effect on the TTV value, which means that a change in the translational amplitude does not greatly affect the surface flatness. For the concave workpiece, when the translational amplitude ranges from 10 to 20 mm, the TTV value decreases with an increase in the translational amplitude. In the translational amplitude range of 20 to 60 mm, the surface flatness has a relatively stable trend, and the amplitude of translation has little effect. In the range of 60 to 70 mm, the TTV value increases with an increase in the translational amplitude.

Figure 12 shows the relationship between the translational velocity and the TTV value of workpiece surfaces with different initial shapes. For a translational speed in the range of 20 to 100 mm/s, the surface flatness and translational speed of surface workpieces of all shapes are in a horizontal linear relationship. This indicates that the translational speed has little
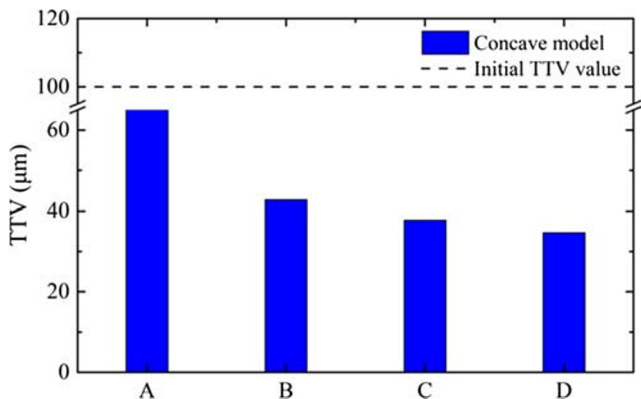
effect on the surface flatness and changing the translational speed minimally affects the surface flatness.

Figure 13 shows the relationship between the polishing gap and the TTV value of workpiece surfaces with different shapes. The TTV value of workpiece surfaces with planar, convex, waved, and pleated shapes decreases with an increase in the polishing gap. This indicates that these four types of workpiece surfaces gradually improve, along with the surface flatness, with decreases in the polishing gap. For the curved workpiece, when the polishing gap is below 2 mm, the TTV value is inversely proportional to the polishing gap. When the polishing gap is above 2 mm, it does not affect the TTV value. For the concave workpiece, the TTV value of the surface flatness does not change with an increase in the polishing gap for the simulation conditions, which indicates that the polishing gap minimally affects this type of workpiece surface flatness.

Figure 14 shows the relationship between the translational direction and the TTV value of workpiece surfaces with different initial shapes. It can be seen from the figure that the workpiece is polished along the X-axis direction and the Y-axis direction along two translational directions, and the curve of the surface flatness TTV value is almost a linear trend. This

Fig. 18 Effect of different magnetic pole arrangements on the TTV value of concave surfaces

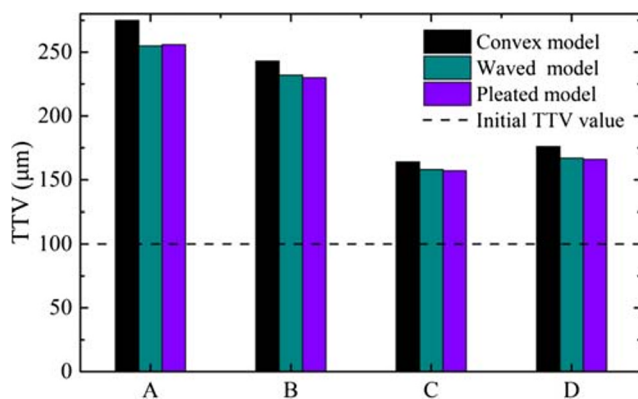Fig. 20 Effect of different magnetic pole arrangements on the TTV Value of convex, waved, and pleated surfaces

Table 3 Processing parameters

Workpiece size (in)	4
Polishing gap (mm)	2
Polishing head speed (r/min)	500
Polishing lap speed (r/min)	10
Magnetic field speed (r/min)	30
Center distance, e_1 (mm)	237.5

indicates that the two translational directions have essentially the same effect on the surface flatness, with little difference between the two.

4.3 Analysis of the effect of the magnetic pole arrangement on the surface flatness

This section aims to study the effect of magnetic field generators, with different magnetic pole arrangements, on the flatness of surfaces with different initial shapes. At the outset, the magnetic field generator models of different magnetic pole arrangements are established, which includes an A-shape with the adjacent arrangement of rectangular anisotropic magnetic poles, a B-shape with the adjacent arrangement of circular anisotropic magnetic poles, a C-shape with the rotating arrangement of cylindrical anisotropic magnetic poles, and a D-shape with the staggered arrangement of cylindrical anisotropic magnetic poles. A magnetic field simulation and analysis is performed by using the Maxwell finite element software to obtain the magnetic field strength of the four types of magnetic field areas. Different magnetic pole arrangement models and magnetic field strength simulations are shown in Figs. 15 and 16.

The prediction model of the workpiece surface flatness is simulated with magnetic field generators of different magnetic pole arrangements. The effect of magnetic field generators with different magnetic pole arrangements on the flatness of surfaces with different initial shapes is analyzed, as shown in Fig. 11. For a certain set of polishing process parameters (w_1 = 500 r/min, w_2 = 20 r/min, w_3 = 20 r/min, A = 40 mm, v = 40 mm/s, translation along the X-axis direction), workpieces with different initial shapes are polished by using magnetic field

Table 4 MRFF composition

Composition	Weight content (%)
Water	21
Carbonyl iron powder	63
Alumina abrasive	10
Glycerol	1.6
Diatomite	1.8
Other additives	2.6

generators with different magnetic pole arrangements. The simulation results are analyzed, as shown in Figs. 17, 18, 19, and 20.

Figure 17 shows that a planar workpiece with an initial TTV value of 0 μm has poor surface flatness after being polished with four types of magnetic pole arrangements. The reason is that the initial shape of the workpiece is perfectly flat, and the polished surface can only be worse. However, the workpiece processed under the magnetic field generator with the C-type magnetic pole arrangement has relatively good surface flatness, and the TTV value reaches about 60 μm. After polishing, the surface flatness is the worst for the C-type magnetic pole arrangement.

Figure 18 shows that after the concave workpiece with an initial TTV value of 100 μm is polished with four types of magnetic pole arrangements, its TTV value is reduced to below 100 μm. This indicates that the four types of magnetic pole arrangements have improved the surface flatness of the concave-shaped workpiece, and the surface shape has been corrected. Among them, the B-type, C-type, and D-type magnetic pole arrangements have similar effects on improving the surface flatness, and the TTV value can be reduced to about 40 μm. The A-type magnetic pole arrangement has the least impact on improving the flatness, which drops from 100 μm to about 75 μm which represents an improvement of 25 μm.

Figure 19 shows that after the curved workpiece with an initial TTV value of 100 μm is polished for the A-type magnetic pole arrangement, its TTV value increased from 100 μm to around 175 μm. For the B-type magnetic pole arrangement, the TTV value increased from 100 μm to around 140 μm. It can be concluded that the surface flatness has not been improved for these two types of magnetic pole arrangements; not only has the surface shape not been corrected, but instead, it has gradually deteriorated. After these two types of workpieces are polished with the C-type and D-type magnetic pole arrangements, the surface flatness TTV value remains around 100 μm, which indicates that the surface flatness has neither improved nor worsened. This shows that after the curved shape workpiece is polished in these two magnetic pole arrangements, it retains the original surface flatness in addition to removing the surface material.

Figure 20 shows that for the four kinds of magnetic pole arrangements, after the convex, waved, and pleated shaped workpieces with an initial TTV value of 100 μm are polished, the variation of the TTV value of the three types of workpieces tends to be consistent, while the TTV value in all cases increases to above 100 μm. This indicates that after the convex, waved, and pleated workpieces are polished under the four types of magnetic field arrangements, the surface flatness will not be improved and will only worsen. Compared with the other two types, the flatness of the polished workpiece is relatively poor for the A and B types of magnetic pole arrangements, and the TTV value is as high as about 250 μm.

Fig. 21 MRPF experiment platform. **a** MRPF experiment equipment. **b** Three-component Kistler dynamometer

(a)　　　　　　　　　　　　　　(b)
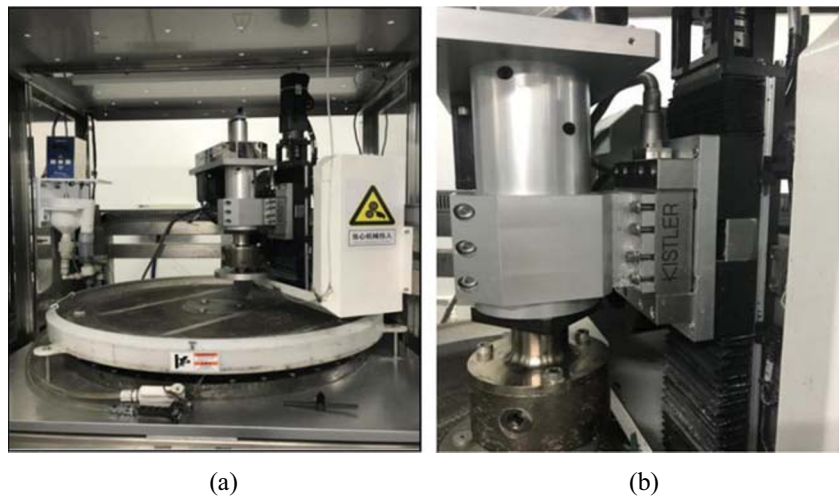
After the workpieces are polished, the surface flatness of the workpieces with different shapes is significantly different for the magnetic field generator with different magnetic pole arrangements. Under different magnetic pole arrangements, the surface flatness of the polished concave workpiece will be improved, and the surface flatness of the polished convex, waved, and pleated workpieces will progressively worsen. Under the C and D types of magnetic pole arrangements, the curved workpiece can maintain the original surface flatness after polishing. Therefore, magnetic field generators with different magnetic pole arrangements can be established for workpieces of different shapes to improve their surface flatness.

5 Experimental procedure and results

Solving for the positive polishing force on the workpiece surface is the basis for establishing the surface flatness prediction
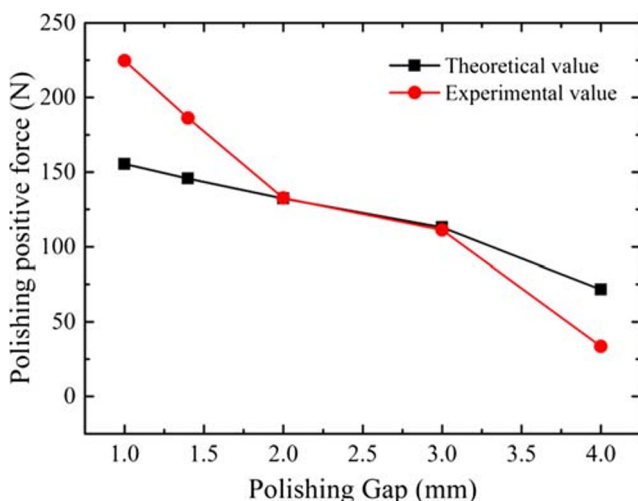
Fig. 22 Polishing positive force

model. Therefore, in this section, the experimental determination of the positive polishing force is described, which verifies the basis of establishing the prediction model of the surface flatness. A gallium arsenide wafer was subjected to magnetorheological polishing on equipment developed for this experiment. The polishing equipment is shown in Fig. 21. The magnetic field generator is D-shaped with a staggered arrangement of cylindrical anisotropic magnetic poles. A 4-in. gallium arsenide wafer was used as the original sample to conduct a magnetorheological plane polishing test. The wafer was cleaned and affixed to the polishing head with wax. The magnetorheological polishing liquid was then poured on to the polishing disk, and the processing gap was 2 mm. The specific process parameters are shown in Table 3, and the composition of the magnetorheological polishing fluid (MRFF) used is shown in Table 4.

A three-component dynamometer was used to measure the magnitude of the positive polishing force on the workpiece surface during magnetorheological plane finishing. The positive polishing force for different processing gaps was obtained, and the experimental data were compared with the results of theoretical simulations. The theoretical and experimental values of the positive polishing force decrease with an increase in the processing gap as shown in Fig. 22. It is also seen that the theoretical and experimental values of the positive polishing force on the workpiece surface are in good agreement. The experimental results thus verify the magnitudes of the positive polishing force obtained from theoretical simulations. The distribution of the positive polishing force is also verified in Fig. 23. The theoretical positive polishing pressure distribution is shown in Fig. 23a, and the actual magnetorheological polishing film is shown in Fig. 23b. It is seen that the distribution of the magnetorheological polishing fluid is the same as the distribution of the theoretical positive polishing force. Therefore, the magnitude and distribution of the positive polishing force on the workpiece surface has been
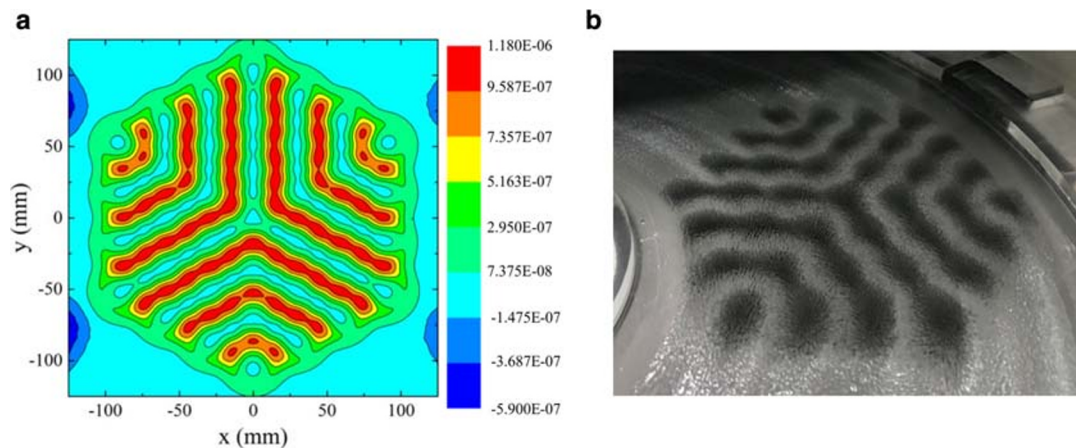
Fig. 23 The distribution map of polishing positive force. **a** The distribution map of theoretical polishing positive force. **b** Magnetorheological polishing film

verified by experimentation, which, in turn, verifies the prediction model for workpiece surface flatness.

6 Conclusions

In this paper, based on MRPF experiments, a prediction model for workpiece surface flatness has been established. The influence of process parameters, such as speed ratio and eccentricity, on the workpiece surface flatness is analyzed, and the effect of multi-pole arrangements on the surface flatness of workpieces with different shapes is explored. The following conclusions are drawn from the results:

1. A method of combining the mechanism of removal of micro-points with the empirical Preston equation can be utilized to establish a prediction model of workpiece surface flatness, which can also be effectively implemented with the prediction models of workpiece surface flatness for other polishing methods.

2. The effects of polishing process parameters (polishing time, speed ratio, translational amplitude, translational speed, etc.) on the surface flatness of workpieces with various surface shapes and an initial flatness of 100 μm have been studied. The results indicate the following: (i) with changes in different process parameters, the surface flatness of the planar, convex, waved, and pleated workpieces tends to be consistent, which is poor after polishing with the worst being about 300 μm; (ii) the change of process parameters has little effect on the overall surface flatness of curved workpieces; and (iii) compared with the other five types of workpieces studied, the improvement of the surface flatness is the most for a concave workpiece after it is polished, which, on average, is about 75 μm and ranges from 100 to 25 μm.

3. After polishing, the surface flatness of workpieces with different shapes and an initial flatness of 100 μm is significantly different when a magnetic field generator with different magnetic pole arrangements is used. For different magnetic pole arrangements, the surface flatness of polished concave workpieces improved from 100 to 30 μm, while the surface flatness of the polished convex, waved, and pleated workpieces progressively worsened, with the worst being about 250 μm. Under the C and D types of magnetic pole arrangements, curved workpieces can maintain the original surface flatness after polishing. A magnetic field generator with different magnetic pole arrangements can thus be established for workpieces of different shapes to improve their surface flatness.

References

1. Zhang P, Dong YZ, Choi HJ, Lee CH, Gao YS (2020) Reciprocating magnetorheological polishing method for borosilicate glass surface smoothness. J Ind Eng Chem 84:243–251. https://doi.org/10.1016/j.jiec.2020.01.004

2. Dai YF, Peng XQ (2013) Overview of key technologies for optical manufacturing of lithographic projection lens. J Mech Eng 49:10–18

3. Huang Y, He S, Xiao GJ, Li W, Jiahua SL, Wang WX (2020) Effects research on theoretical-modelling based suppression of the contact flutter in blisk belt grinding. J Manuf Process 54:309–317. https://doi.org/10.1016/j.jmapro.2020.03.021

4. Luo B, Yan Q, Pan J, Guo M (2020) Uniformity of cluster magnetorheological finishing with dynamic magnetic fields formed by multi-magnetic rotating poles based on the cluster principle. Int J Adv Manuf Technol 107:919–934. https://doi.org/10.1007/s00170-020-05088-1

5. Parameswari G, Jain VK, Ramkumar J, Nagdeve L (2019) Experimental investigations into nanofinishing of Ti6Al4V flat disk using magnetorheological finishing process. Int J Adv Manuf Technol 100:1055–1065. https://doi.org/10.1007/s00170-017-1191-3

6. Guo CW, Chen F, Meng QR, Dong ZX (2014) Yield shear stress model of magnetorheological fluids based on exponential distribution. J Magn Magn Mater 360:174–177. https://doi.org/10.1016/j.jmmm.2014.02.040

7. Chen MJ, Liu HN, Cheng J, Yu B, Fang Z (2017) Model of the material removal function and an experimental study on a magnetorheological finishing process using a small ball-end permanent-magnet polishing head. Appl Opt 56:5573–5582. https://doi.org/10.1364/AO.56.005573

8. Wang YY, Zhang Y, Feng ZJ (2016) Analyzing and improving surface texture by dual-rotation magnetorheological finishing. Appl Surf Sci 360:224–233. https://doi.org/10.1016/j.apsusc.2015.11.009

9. Kordonski W, Gorodkin S (2011) Material removal in magnetorheological finishing of optics. Appl Opt 50:1984–1994. https://doi.org/10.1364/AO.50.001984

10. Catrin R, Neauport J, Taroux D, Cormont P, Maunier C, Lambert S (2014) Magnetorheological finishing for removing surface and subsurface defects of fused silica optics. Opt Eng 53(0920109):092010. https://doi.org/10.1117/1.OE.53.9.092010

11. Saraswathamma K, Jha S, Rao PV (2015) Experimental investigation into ball end magnetorheological finishing of silicon. Precis Eng 42:218–223. https://doi.org/10.1016/j.precisioneng.2015.05.003

12. Dai YF, Song C, Peng XQ, Shi F (2010) Calibration and prediction of removal function in magnetorheological finishing. Appl Opt 49:298–306

13. Kumar S, Singh AK (2018) Nanofinishing of BK7 glass using a magnetorheological solid rotating core tool. Appl Opt 57:942–951. https://doi.org/10.1364/AO.57.000942

14. Pan JQ, Yu P, Yan QS (2018) Experimental investigations on the polishing forces characteristics of dynamic magnetic field magnetorheological effect polishing pad. J Mech Eng 54:10–17

15. Wang YQ, Yin ZH, Li YP, Hu T, Chen FJ (2017) Effects of translational movement on surface planarity in magnetorheological planarization process. J Mech Eng 53:206–214. https://doi.org/10.3901/JME.2017.01.206

16. Zhang YF, Fang FZ, Huang W, Wang C, Fan W (2018) Polishing technique for potassium dihydrogen phosphate crystal based on magnetorheological finishing. Procedia CIRP 71:21–26. https://doi.org/10.1016/j.procir.2018.05.012

17. Fang CF, Zhao ZX, Lu LY, Lin YF (2016) Influence of fixed abrasive configuration on the polishing process of silicon wafers.

18. Int J Adv Manuf Technol 88(1–4):1–10. https://doi.org/10.1007/s00170-016-8808-9

Krishnan M, Nalaskowski JW, Cook LM (2010) Chemical mechanical planarization: slurry chemistry, materials, and mechanisms. Chem Rev 110:178–204. https://doi.org/10.1021/cr900170z

19. Nie M, Cao JG, Liu YM, Li JY (2018) Influence of magnets' phyllotactic arrangement in cluster magnetorheological effect finishing process. Int J Adv Manuf Technol 99:1699–1712. https://doi.org/10.1007/s00170-018-2603-8

20. Guan F, Hu H, Li SY, Liu ZY, Peng XQ, Shi F (2018) A novel lap-MRF method for large aperture mirrors. Int J Adv Manuf Technol 95:4645–4657. https://doi.org/10.1007/s00170-017-1498-0

21. Zou YH, Jiao AY, Aizawa T (2010) Study on plane magnetic abrasive finishing process-experimental and theoretical analysis on polishing trajectory. Adv Mater Res 126–128:1023–1028. https://doi.org/10.4028/www.scientific.net/amr.126-128.1023

22. Lu JB, Yan QS, Pan JS, Gao WQ (2012) Experiments of synergistic effect of electro-magnetically coupled field in EMR finishing. Opt Precis Eng 20:2485–2491

23. Pan J, Yan Q (2015) Material removal mechanism of cluster magnetorheological effect in plane polishing. Int J Adv Manuf Technol 81(9–12):2017–2026. https://doi.org/10.1007/s00170-015-7332-7

24. Jha S, Jain VK (2006) Modeling and simulation of surface roughness in magnetorheological abrasive flow finishing (MRAFF) process. Wear 261:856–866. https://doi.org/10.1016/j.wear.2006.01.043

25. Pan JS, Yan QS, Xu XP, Zhu JT, Wu ZC, Bai ZW (2012) Abrasive particles trajectory analysis and simulation of cluster magnetorheological effect plane polishing. Phys Procedia 25:176–184. https://doi.org/10.1016/j.phpro.2012.03.067

26. Zhao DW, Wang TQ, He YY, Lu XC (2013) Kinematic optimization for chemical mechanical polishing based on statistical analysis of particle trajectories. IEEE Trans Semicond Manuf 26:556–563. https://doi.org/10.1109/TSM.2013.2281218

27. Rastegar V (2018) Effect of large particles during chemical mechanical polishing based on numerical modeling of abrasive particle trajectories and material removal non-uniformity. IEEE Trans Semicond Manuf 31:277–284. https://doi.org/10.1109/TSM.2018.2796564